ADVANCED FUNCTIONAL MATERIALS
www.afm-journal.de

Fundamental Tradeoff between Emission Intensity and Efficiency in Light-Emitting Electrochemical Cells

*Stephan van Reenen, René A. J. Janssen, and Martijn Kemerink**

The characteristic doping process in polymer light-emitting electrochemical cells (LECs) causes a tradeoff between luminescence intensity and efficiency. Experiments and numerical modeling on thin film polymer LECs show that, on the one hand, carrier injection and transport benefit from electrochemical doping, leading to increased electron-hole recombination. On the other hand, the radiative recombination efficiency is reduced by exciton quenching by polarons involved in the doping. Consequently, the quasi-steady-state luminescent efficiency decreases with increasing ion concentration. The transient of the luminescent efficiency shows a characteristic roll-off while the current continuously increases, attributed to ongoing electrochemical doping and the associated exciton quenching. Both effects can be modeled by exciton polaron-quenching via diffusion-assisted Förster resonance energy transfer. These results indicate that the tradeoff between efficiency and intensity is fundamental, suggesting that the application realm of future LECs should be sought in high-brightness, low-production cost devices, rather than in high-efficiency devices.

1. Introduction

The unique selling point of light-emitting electrochemical cells (LECs) is the fact that a single active layer that enables both ionic and electronic conduction can perform the tasks of injection, transport, and recombination of electrons and holes.[1,2] Upon application of a sufficiently large electrical bias ions and electronic charges redistribute to effectively form a five-layer device with injection and doped transport layers for electrons and holes sandwiching an intrinsic recombination zone.[2,3] Despite significant efforts aimed at improving the performance and the understanding of LECs, their luminous efficiency has remained moderate (20 lm W^{-1} for best reported white LEC[4] compared with multilayer organic light emitting diodes (OLEDs) (114 lm W^{-1} for best reported white OLED[5]. In view of the well-established excellent injection and transport characteristics of LECs this is surprising. To determine and possibly remove the origin of the limited performance of LECs, the conversion from electrical current into radiatively decaying excitons must be fully understood.

The current-to-light conversion occurs through multiple steps, starting from recombination of carriers into excitons, followed by exciton decay, and outcoupling of the generated light. As for the first step, the presence in well-functioning LECs of a stable intrinsic recombination zone between high-density p- and n-type doping zones[2,3] ensures balanced hole and electron currents[6] and a close to unity recombination efficiency.[7] As for the last step, the light outcoupling in LECs is expected to be similar to that in OLEDs. Hence, the relatively low efficiency of LECs compared with OLEDs is most likely related to nonradiative exciton decay.

Indeed, the radiative efficiency of the operational LECs remains typically well below the (fine) PL efficiency of the emissive species used, both for LECs based on polymers[8] and on ionic transition metal complexes (iTMCs).[7] Various nonradiative decay processes can in principle be responsible for this. Quenching of excitons may be induced by the large density of polarons in the doped regions.[9] Additionally, exciton–exciton interactions may be expected as a high concentration of excitons is formed in the relatively narrow intrinsic zone. Also impurities in the active layer, e.g., related to the electrolyte, may give rise to further reduction of the radiative fraction.

A strong indication that excitons are quenched by polarons in LECs is the typical roll-off in efficiency for both polymer- and iTMC-based LECs.[10] This roll-off occurs while the current density continues to increase, which indicates continuous electrochemical doping. This slow doping process was previously attributed to slow dissociation of salt into mobile ions that subsequently can be used in doping.[3] In fact, in a number of recent papers doping-related quenching was proposed as cause for the efficiency roll-off.[11–13] Formal justification of this assignment is however lacking.

Here, we investigate the difference in efficiency in LECs compared with OLEDs based on the same organic semiconductor. The origin of the efficiency roll-off in LECs is studied in detail as well as the influence of the admixed salt concentration c_0 in the active layer on the quasi-steady-state electroluminescent efficiency. Experiments show a strong reduction

Dr. S. van Reenen, Prof. R. A. J. Janssen, Prof. M. Kemerink
Department of Applied Physics
Eindhoven University of Technology
P.O. Box 513, 5600 MB, Eindhoven, The Netherlands
E-mail: martijn.kemerink@liu.se
Prof. R. A. J. Janssen
Department of Chemical Engineering
Eindhoven University of Technology
P.O. Box 513, 5600 MB Eindhoven, The Netherlands
Prof. M. Kemerink
Department of Physics
Chemistry and Biology (IFM)
Linköping University
SE-58183 Linköping, Sweden

DOI: 10.1002/adfm.201403945

© 2015 WILEY-VCH Verlag GmbH & Co. KGaA, Weinheim

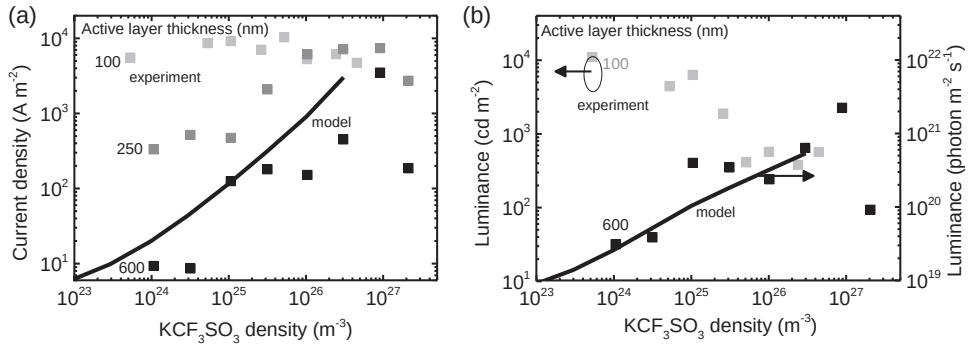

Figure 1. Experimentally (symbols, V_{bias} = 8 V) and numerically (lines, V_{bias} = 3.5 V) determined quasi-steady-state current density a) and luminance b) of LECs. The active layer thicknesses of the experimental ITO/PEDOT:PSS/SY-PPV:PEO:KCF_3SO_3 = 5:1:*x*/LiF/Al devices is indicated. No luminance measurements were performed on the 250 nm cells. The thickness of the modeled LEC was 100 nm.

in quasi-steady-state efficiency for increasing c_0. Additionally, transient characterization of these devices displays the typical roll-off in efficiency during electrochemical doping. The data is reproduced by numerical modeling to constitute that, compared with OLEDs, the efficiency in LECs is limited by polaron-induced exciton quenching. These results point toward a fundamental tradeoff in LECs between charge transport, with more doping giving rise to higher current densities and even higher emission intensities, and radiative decay, with polarons involved in the doping opening a nonradiative decay channel.

2. Results and Discussion

The luminescent efficiency of polymer LECs is experimentally investigated by measurement of the transient luminescent efficiency and quasi-steady-state luminescent efficiency in devices with varying doping concentrations. The doping concentration is altered by variation of the admixed salt density c_0. Simulations to complement the experiments were performed by a numerical drift-diffusion model. Details are described in the Experimental Section and Section A of the Supporting Information.

2.1. Steady-State Operation

To avoid studying injection limited devices at low c_0, LECs were prepared with low work function cathodes, LiF/Al, and high work function anodes, ITO/PEDOT:PSS, to enable ohmic injection in the semiconductor, a phenyl-substituted poly(*p*-phenylene vinylene) copolymer commonly termed "Super Yellow" (SY-PPV). The (limited) effect of using different electrode materials is shown in the Supporting Information Section B. The active layer consisted of SY-PPV: Poly(ethylene oxide) (PEO) in a fixed weight ratio of 5:1 and a variable amount x (for $x = 2 \times 10^{-4}$–0.6) of salt, KCF_3SO_3, resulting in an average salt density between $\approx 10^{24}$ and $\approx 10^{27}$ m^{-3}. The salt density was determined from these weight ratios, the molecular mass of the constituents and assuming a density of 1 g cm^{-3} in the active layer. Several series of LECs were studied with varying active layer thickness L of 100 ± 10, 250 ± 25 and 600 ± 40 nm. The latter two series were prepared by spin-coating subsequent layers on top of each other.[14] Care was taken that any previous layers were dry before depositing the next layer. The devices were electrically characterized by subsequent voltage sweeps up to 8 V. During these sweeps, the current density was found to converge to a single quasi-steady-state value at 8 V. Similar voltage sweeps up to lower bias voltages resulted in hysteresis in subsequent sweeps, i.e., a continuous increase in the current density at the maximum bias voltage, indicating that a quasi-steady-state situation had not been reached. For the 8 V scans, electrochemical side-reactions were not observed by eye, nor was there any indication of this in the relatively fast *I*–*V* sweeps as the current density at 8 V was not observed to decrease for subsequent scans. For *I*–*V* sweeps with a maximal voltage above 8 V, such reductions in current density were observed. Prolonged operation at 8 V, unlike the *I*–*V* sweeps mentioned here, did however also result in degradation of the device. The current density and luminance at 8 V are plotted for all three series in **Figure 1**a,b.

To enable qualitative comparison with the experiments, the results of simulations of the steady-state current density and luminance of an LEC biased at 3.5 V are shown in Figure 1a,b. Here L is 100 nm and a constant electronic carrier mobility is assumed. A constant mobility was taken to keep the calculation time within reasonable limits and to avoid the addition of too many parameters. Addition of such a doping dependent mobility would lead to an even stronger enhancement of the current as a function of doping density than the enhancement shown in Figure 1a. Due to long calculation times, only a single device thickness (L) was modeled. Given the constant electronic carrier mobility, variation of L between 100 and 600 nm would mainly result in enlargement of the doped regions and the supply of carriers toward the recombination zone would remain similar. Therefore, only minor quantitative differences are expected upon varying L. A diffusion-assisted polaron-induced exciton-quenching model was implemented in the model as described in the Experimental Section. The following parameters related to the excitons were set to values obtained from literature: the radiative decay rate $k_{decay} = 1/\tau_D^\circ = 1.54$ ns^{-1} found in SY-PPV and the exciton diffusion coefficient $D_{ex} = 3 \times 10^{-8}$ m^2 s^{-1} found in the related NRS-PPV.[15,16] The Förster critical radius R_0 was set at 3 nm. This value is similar to the values obtained in ref.[9] for p- and n-type doping of SY-PPV of 2.8 ± 0.6 and 2.3 ± 0.4 nm, respectively. These were determined from the polaron absorption and excitation spectra.

© 2015 WILEY-VCH Verlag GmbH & Co. KGaA, Weinheim

As expected, the simulations show that an enhancement of the salt density results in an enhancement of the current density. The luminance increases accordingly. This is related to the ability of the device to prevent space charge formation while accumulating larger densities of mobile charge carriers in the active layer through electrochemical doping.[12,17] For the thicker LECs (L = 250 and 600 nm) an enhancement of the current density is also experimentally observed for increasing salt density. For the 600 nm device, the luminance is also observed to be enhanced. No luminance measurements were performed for the 250 nm devices. For the series with L = 100 nm, surprisingly a current density is observed that is nearly independent of the admixed salt density. Apparently, carrier transport cannot be further enhanced in these 100 nm-thick LECs, probably due to a cancelation of various factors. The luminance is however reduced, which is rationalized below.

The efficiency of the experimental and simulated LECs (see Figure 1) is plotted in **Figure 2**. The dashed lines indicate the experimentally determined efficiency of OLEDs with layer stacks ITO/PEDOT:PSS/SY-PPV/LiF/Al and ITO/PEDOT:PSS/SY-PPV:PEO (5:1 in w%)/LiF/Al. The efficiency of these OLEDs is highly similar, indicating that the inclusion of PEO hardly affects the efficiency. It is also similar to the efficiencies measured in the LECs at relatively low c_0. The efficiency of the 100 and 600-nm thick LECs in Figure 2 (symbols) is reduced by an order of magnitude by increasing the salt density from ≈10^{24} to ≈10^{27} m^{-3}.

In the numerical modeling, excitons can either decay radiatively or be quenched by electrons or holes. The efficiency of the modeled LEC is plotted in Figure 2 for varying exciton diffusion coefficients ($D_{ex} = 3 \times 10^{-8}$ m^2 s^{-1} was experimentally determined in NRS-PPV, which is structurally and electro-optically comparable to SY-PPV).[16] The modeled results (in lines and symbols in Figure 2) lie more or less in between the experimentally obtained efficiency values (symbols in Figure 2). The maximal efficiency of the model (0.25 photon/electron) is set at the same position on the vertical axis as the experimentally determined efficiency of the salt-free OLEDs (dashed lines). This procedure is used to effectively account for the absence of other nonradiative loss channels and outcoupling effects in our simulations. Importantly, the same y-axis scale on left and right assures that *relative* salt-induced changes can be one-on-one compared.

The qualitative and quantitative agreement between model and experiment strongly suggests that polaron-induced exciton quenching can indeed dominate the efficiency reduction in polymer LECs. Note that all relevant parameters in the model have been independently determined or were taken from literature, so that the agreement does not rely on any fitting. On top of polaron-induced exciton quenching also doping-induced self-absorption has recently been shown to lead to a reduced output of electroluminescence in LECs during operation.[13]

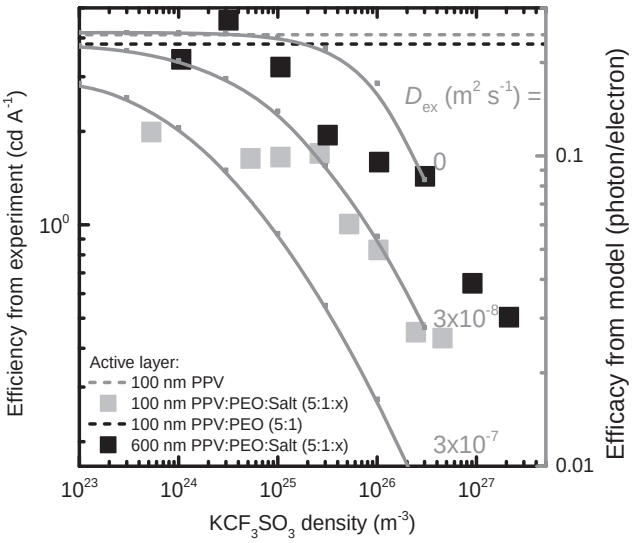

Figure 2. Experimentally (squares, V_{bias} = 8 V) and numerically (lines and symbols, V_{bias} = 3.5 V) determined efficiency in LECs versus admixed KCF_3SO_3 density. The dashed lines indicate the efficiency in absence of KCF_3SO_3. The legend indicates the active layer composition for the experiments, which is sandwiched between ITO/PEDOT and LiF/Al electrodes. The exciton diffusion coefficients in m^2 s^{-1} are indicated for each numerical calculation.

2.2. Transient Operation

Another route to determine the origin of the reduced luminescent efficiency in LECs is by study of the transient behavior. As already shown for different types of LECs,[10] after application of a constant, above-bandgap bias voltage the LECs show a characteristic roll-off of the efficiency while the current density continues to increase. In the LECs studied here, this characteristic is also observed as shown in **Figure 3**. The current, luminance,

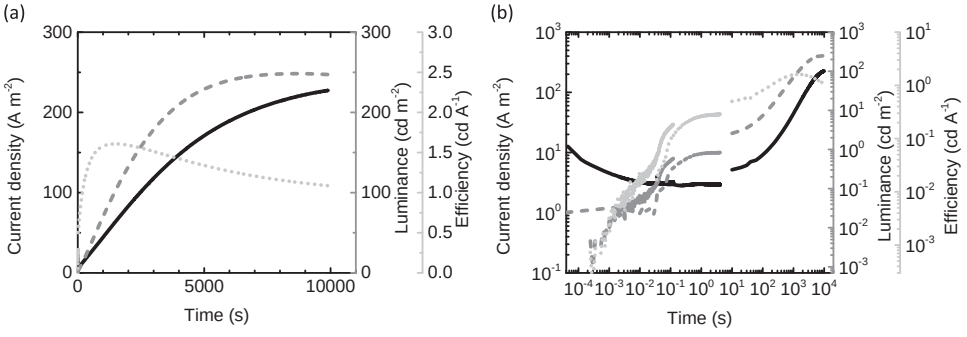

Figure 3. Experimentally determined transients of the current density (solid line), luminance (dashed lines), and efficiency (dotted lines) in an ITO/PEDOT:PSS/SY-PPV:PEO:KCF_3SO_3 (=100:20:1, i.e., $c_0 = 1.3 \cdot 10^{25}$ m^{-3})/LiF/Al LEC with L = 230 nm and V_{bias} = 5 V. (a) and (b) show the same results on linear and logarithmic scales, respectively.

© 2015 WILEY-VCH Verlag GmbH & Co. KGaA, Weinheim

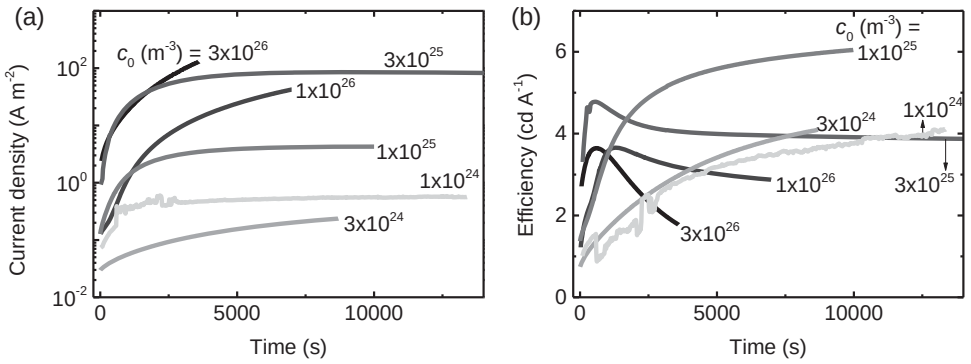

Figure 4. Experimentally determined transients of a) the current density and b) the efficiency of a ITO/PEDOT:PSS/SY-PPV:PEO(5:1)+ KCF_3SO_3/LiF/Al LEC with $L \approx 600$ nm and $V_{bias} = 6$ V. The admixed KCF_3SO_3 density c_0 is indicated at each graph.

and efficiency were characterized in three subsequent measurements on different timescales as shown in Figure 3b. Due to the disabling of the bias voltage in between, the transients do not connect perfectly, but they do show the general behavior of the LEC over eight orders in time. Transients below $\approx 10^0$ s were observed to be qualitatively reproducible with the same LEC, as deduced from repetitive measurements. Quantitatively minor differences occur nevertheless as visible in Figure 3b. Prolonged operation for $t > 10^1$ s however typically changes the LECs irreversibly, presumably due to remnant doping which does not relax within at least several hours.

Also in transient experiments, enhancement of c_0 results in enhanced quenching as shown in **Figure 4**. Like in Figure 1 the current density shows a clearly increasing trend with increasing c_0, at the cost of efficiency. Roll-off in the efficiency transients is observed for $c_0 > 10^{25}$ m^{-3}, with lower (near) saturation efficiencies for larger c_0. The relatively low efficiency for the devices with a low c_0, i.e. 1×10^{24} and 3×10^{24} can be attributed to a relatively long stabilization time compared with devices with higher values of c_0.

To complement the experiments, the numerical model was used to calculate current, luminance (see Section C of the Supporting Information), and efficiency transients in LECs. In case only free ions are considered in the model the transients represented by the dashed lines in **Figure 5**b,d are obtained. Neither a large transient enhancement in current density nor a roll-off in efficiency is observed. Although the current density does increase for $10^{-4} < t$ (s) $< 2 \times 10^{-3}$, the timescale on which this happens is very short compared with transients shown in Figure 3b. Clearly, a key ingredient is missing in this description of the LECs. This transient however does resemble the transients typically observed in planar LECs as shown for example in ref.[2]

In ref.[3], we found that the inclusion of anion–cation pairs, i.e., salt, with a binding energy E_s enables a good description of the transient behavior of the electronic current density in thin film LECs. Next to the binding energy, also the capture coefficient γ_c of anions and cations is a free parameter as described in Section A.4 of the Supporting Information. Introduction of bound anion–cation pairs in the model used here significantly changes the transients as demonstrated in Figure 5 for varying E_s and γ_c. The transients in Figure 5 are from LECs which at $t = 0$ are in equilibrium regarding salt association and dissociation. E_s therefore determines the initial fraction of mobile ions of the total salt density c_0. The turn-on transients of LECs with varied E_s (γ_c was changed so as to keep the salt dissociation coefficient $\gamma_d = \gamma_c \exp(E_s/kT)$ constant) is shown in Figure 5a,c. They show, as expected, that for a large initial mobile ion fraction, the initial current is relatively large. Turn-on of light emission is observed around $t \approx 10^{-4}$ s which indicates that the first electrons and holes have traversed the device. This time is related to the carrier mobility and the externally applied electric field. Simultaneously, electrochemical doping takes place by association of free charges with mobile ions. Dissociation of bound anion–cation pairs takes place as well, enabling further electrochemical doping. As salt dissociation is the slowest process, it limits the evolution of the turn-on transient. Simulations for different capture coefficients γ_c and a fixed $E_s = 0.54$ eV are shown in Figure 5b,d. Reduction of γ_c mainly slows down the doping process and enhances the time needed to reach steady-state accordingly. Due to long calculation times steady-state was not reached in these simulations, but the transients should converge to the same final state. The reason is that at steady-state all ions are completely separated from each other and have a fixed density profile due to the contacts which block ion transport. As a consequence, only the density of ions is of importance for steady-state operation of the modeled LEC,[2] not the mobility, the binding energy, or the capture coefficient.

Looking at the transient efficiency of the calculated LECs in Figure 5c,d, a slow roll-off is observed on the same timescale as the current increase—both result from the slow ion dissociation enabling the ongoing doping process. In **Figure 6**, the simulation for $E_s = 0.42$ eV and $\gamma_c = 3 \times 10^{-17}$ m^3 s^{-1} is plotted on a linear and logarithmic scale. Qualitatively, the experimental and calculated transients in Figures 3,6 display the same features. In the modeling (experimental) results, the onset of luminance is observed at 10^{-4} s (10^{-3} s) followed by a relatively constant current density until 10^{-2} s (10^1 s). Current density and luminance subsequently continue to increase, whereas the efficiency reaches its peak-value and rolls off.

In the experiment (Figure 3), additional steps in the efficiency and luminance are observed between 10^{-3} s $< t < 10^3$ s before the maximal efficiency is reached, which are not reproduced by the numerical model. The first step at $\approx 10^{-1}$ s may be related to initial imbalanced charge transport due to a difference in electron and hole mobility, resulting in recombination near one of

© 2015 WILEY-VCH Verlag GmbH & Co. KGaA, Weinheim

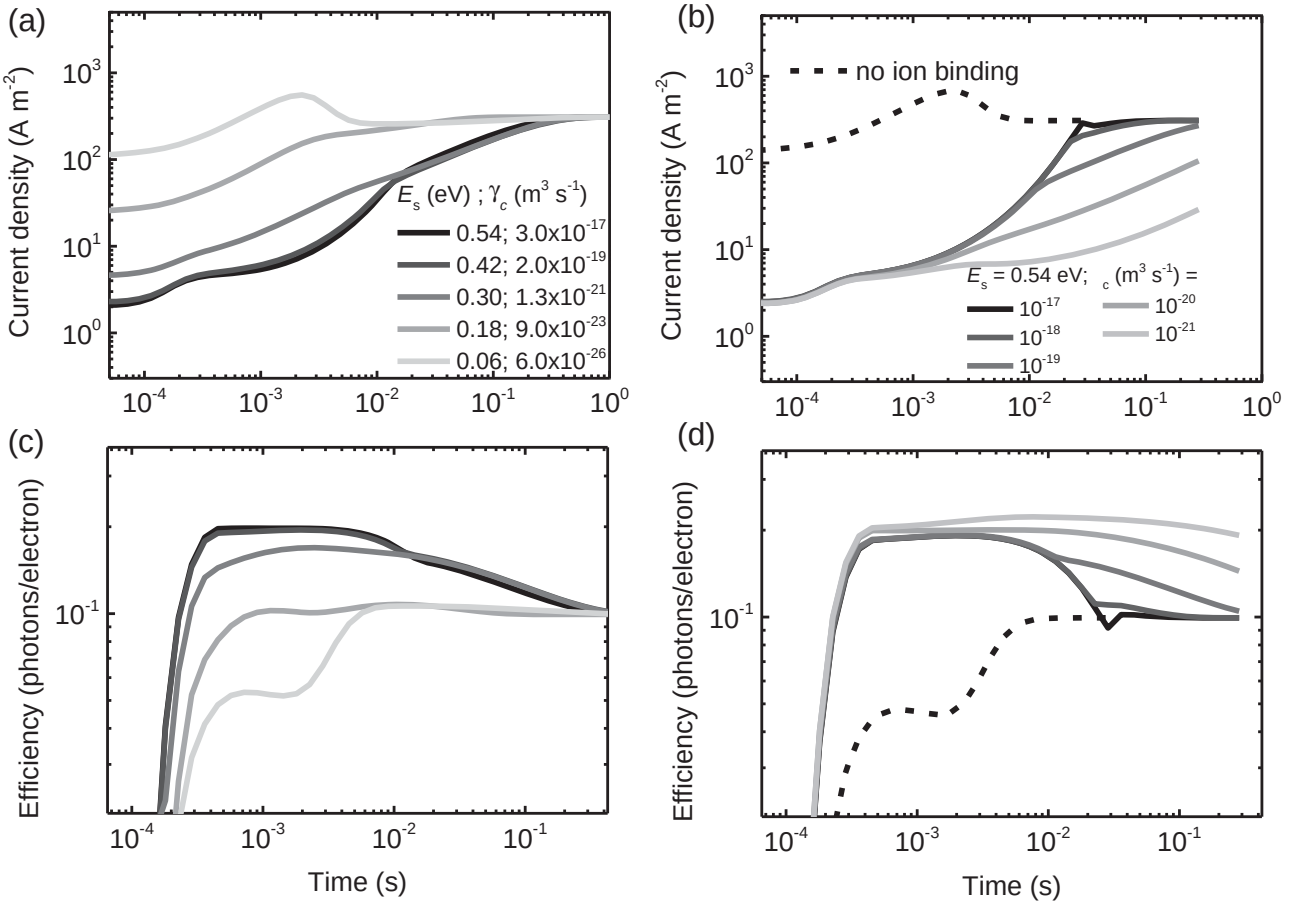

Figure 5. Calculated current density and efficiency transients for varying salt binding parameters a,c) E_s, and γ_c (γ_c was varied in such a way to maintain a constant salt dissociation coefficient, $\gamma_d = \gamma_c \cdot \exp(E_s/kT)$, which essentially results in the majority of salt dissociation to occur between $10^{-3} < t < 10^{-1}$). b,d) γ_c as indicated in the legend. The dashed lines represent a calculation where no associated salt complex can be formed. The salt density is 3×10^{25} m^{-3} and the applied bias voltage 3.5 V.

the contacts followed by exciton quenching due to the contact. In the model, equal carrier mobilities were chosen. Note that after significant electrochemical doping, the recombination efficiency is expected to be ≈100% and recombination is expected to take place further away from the contacts. The increase in efficiency at ≈10^2 s is possibly related to a reduced importance of nonradiative trap-assisted recombination.[18] At relatively high current densities, these traps are saturated so their relative effect on recombination is reduced. Consequently, the efficiency is raised at higher current densities. This may also explain why the efficiency is reduced for the lowest ion densities in Figure 2,4b. Trap-related nonradiative exciton decay processes were not taken into account by the model to not obscure the calculated trends due to polaron-induced exciton quenching.

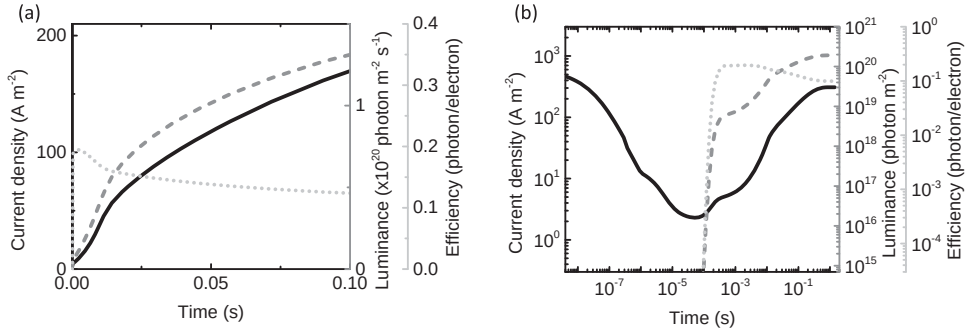

Figure 6. Calculated transients of the current density (solid), luminance (dashed), and efficiency (dotted) in a modeled LEC with ohmic contacts, an $L = 100$ nm, $c_0 = 3 \times 10^{25}$ m^{-3}, $V_{bias} = 3 \times 5$ V, $\mu_{ion} = 10^{-12}$ m^2 V^{-1} s^{-1}, $\mu_{p/n} = 10^{-11}$ m^2 V^{-1} s^{-1}, $E_s = 0.42$ eV, and $\gamma_c = 3 \times 10^{-17}$ m^3 s^{-1}. a) and b) shows the same results on linear and logarithmic scales, respectively.

© 2015 WILEY-VCH Verlag GmbH & Co. KGaA, Weinheim

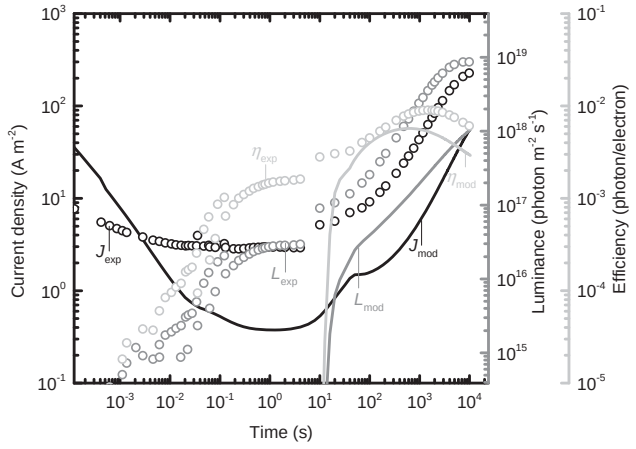

Figure 7. Calculated (lines) and experimental (symbols) transients of current (black), luminance (gray), and efficiency (light gray) of 200, and 230-nm thick LECs biased at 5 V. The time of the numerical data was corrected by a factor 2×10^3.

The transients in Figure 6 are qualitatively similar to the transients in Figure 3. For a more quantitative agreement, some parameters can be modified. The Supporting Information (Section D) discusses in detail how these parameters were chosen and their relation to experiments.

Due to extremely long calculation times a simulation with the expectedly optimal parameters could not be performed. However, for $\mu_{ion} = 10^{-12}$ instead of $\approx 10^{-15}$ m^2 V^{-1} s^{-1} a simulation was carried out, shown in **Figure 7** as lines. Note that the numerical model does not take into account the radiative efficiency related to the non-unity PL quantum yield of SY-PPV, which is 17%,[15] nor the out-coupling efficiency, which is approximately 20% in the experiment. Therefore, to enable good comparison with the experiments, the luminance and the efficiency are multiplied by 0.2×0.17. The experimental results from Figure 3 are included as symbols. The experimental data related to the luminance and the efficiency were converted from cd m^{-2} and cd A^{-1} to photon m^{-2} s^{-1} and photon per electron, respectively, by two related conversion factors. The conversion factor from cd m^{-2} to photon m^{-2} s^{-1} is derived in Section E of the Supporting Information and was found to be 3.5×10^{16} photon cd^{-1} s^{-1}. From this value, the conversion factor from cd A^{-1} to photon per electron follows as 0.0056 photon A cd^{-1} per electron. To enable comparison of the transients during electrochemical doping in model and experiment, the horizontal axis of the modeled results was shifted to compensate for the enhanced ion mobility used in the model. Here, we found that the scaling factor is approximately 2×10^3 which means that, based on the fit, the ion mobility in the experiment is roughly 5×10^{-16} m^2 V^{-1} s^{-1}. Electrochemical doping in Figure 7 takes place at $10^{-1} < t < 10^4$. During this time, the current, luminance, and efficiency transients show quantitative agreement between model and experiment within an order of magnitude. Given the complexity of the system we consider this very satisfactory.

The results of the transient (see Figure 7) and steady-state (see Figures 1,2) operation of polymer LECs has shown that polaron-induced exciton quenching can be considered as one of the main processes, which result in a reduction of the electroluminescent efficiency. Requirements for effective polaron-induced exciton quenching are i) exciton formation near a high density of polarons, ii) exciton diffusion, iii) spectral overlap for exciton emission and polaron absorption, and iv) a sufficient exciton lifetime.[9,19] To avoid exciton quenching, one or more of these requirements should not be fulfilled. Modification of the properties of the conjugated polymer is challenging as it should then be optimized simultaneously for both charge transport and luminescent efficiency, at the required bandgap. To circumvent this, for example dyes can be considered. Qian et al.[20] recently reported on a quantum dot LEC reaching a similar luminescent efficiency as a multilayer quantum dot OLED, despite the presence of some efficiency roll off. Further optimization of such systems may lead to efficient, single layered electroluminescent devices, combining the high efficiencies of OLEDs and the easy processing of LECs.

3. Conclusions

The emission intensity increase and efficiency reduction in polymer LECs due to electrochemical doping have been systematically studied in experiments by investigation of the transient and quasi-steady-state performance. Enhancement of the salt density in polymer LECs is found to reduce the efficiency for admixed salt densities $>10^{25}$ m^{-3}. This reduction in efficiency was successfully reproduced by numerical modeling of LECs in which the only nonradiative loss channel of excitons was quenching by polarons involved in doping. Also the transient efficiency roll-off, typical for many types of LECs, was reproduced by the model. The roll-off is caused by ongoing doping that is enabled by the slow dissociation of salt into mobile ions that subsequently are used to further dope the semiconductor. Hence, the current continues to increase while the efficiency rolls off.

The results show that the ions, which enable electrochemical doping improve electrical transport and concomitantly electron-hole recombination in polymer LECs at the cost of the luminescent efficiency. This tradeoff seems fundamental in nature, suggesting that the application realm of future LECs should be sought in high-brightness, low-production cost devices, rather than in high-efficiency devices.

4. Experimental Section

Device Preparation: The conjugated polymer used in the active layer of the sandwich LECs is a phenyl-substituted poly(*p*-phenylene vinylene) copolymer (SY-PPV, Merck, catalogue number PDY-132), commonly termed "Super Yellow". Poly(ethylene oxide) (PEO, $\bar{M}_w = 5 \times 10^5$ g mol^{-1}, Aldrich) was used as received. The salt potassium trifluoromethanesulfonate (KCF_3SO_3, 98%, Aldrich) was dried at a temperature $T = 373$ K under vacuum before use. SY-PPV (5 mg mL^{-1}), PEO (10 mg mL^{-1}), and KCF_3SO_3 (20 mg mL^{-1}) were dissolved in cyclohexanone (>99%, anhydrous, Aldrich). These solutions were mixed together in varying weight ratios. The resultant stock solutions were thereafter stirred on a magnetic hot plate at $T = 323$ K for at least 5 h. Cleaned glass-ITO substrates were first spin coated with poly(3,4-ethylenedioxythiophene)-poly(styrenesulfonate) (PEDOT:PSS, Clevios P VP AI 4083) from Heraeus (at 2000 RPM for 60 s) and subsequently transferred to a glovebox under N_2 atmosphere ($[O_2] < 1$ ppm and $[H_2O] < 1$ ppm), where the substrates were annealed for 10 min at

© 2015 WILEY-VCH Verlag GmbH & Co. KGaA, Weinheim

120 °C. All the next steps were done in a glovebox. Subsequently, the stock solution was spin coated (in general at 1000 RPM for 60 s) after which, the samples were dried at $T = 323$ K for at least 2 h on a hot plate. Then the substrates were transferred to a thermal evaporator, where LiF/Al or Al electrodes were deposited by thermal evaporation under high vacuum ($p \approx 10^{-6}$ mbar) on top of the spin-coated films. The active areas of the devices, defined by a shadow mask, were either 0.091 or 0.161 cm^2. The thickness of the active layers was measured after complete electrical characterization by profilometry in air.

Electrical Characterization: Current–luminance–voltage characteristics were measured by a Keithley 2636a sourcemeter and a silicon photodiode. The brightness was calibrated with a luminance meter (LS-110 Konica-Minolta). In general, two types of measurements were performed. Current and luminance were measured while sweeping the bias voltage V_{bias}. To achieve reproducible *I–V* curves, three subsequent voltage sweeps were performed typically from 0 to 8 to 0 V in ≈20 s. In addition, the current and luminance were also measured as a function of time at a constant bias voltage of 6 V. To achieve the short-timescale measurement as shown in Figure 3b (for $t < 10^{-1}$ s), the Analog/Digital converter speed of the Keithley 2636a sourcemeter was reduced to 0.001 number of power line cycles. Consequently, there is slightly more noise in the signal.

Computational Details: For the numerical simulations, a 2D drift-diffusion model was used,[21] which is described in detail in Section A of the Supporting Information. Here follows a general description of the used parameters. Deviating parameters are mentioned where necessary. The model was used to describe a 1D device with constant grid-point spacing of 2 nm and a total active layer thickness of 100 nm. The carrier mobility was chosen to be field and doping independent and set to $\mu_{p/n} = 10^{-11}$ m^2 V^{-1} s^{-1} unless stated otherwise. The anion and cation mobilities were chosen to be $\mu_{ion} = 10^{-12}$ m^2 V^{-1} s^{-1}. The ion mobility at the interface layer at the contacts was set to zero to prevent accumulation at the electrodes. If not, an unphysically large number of ions would pile up next to the electrodes and be completely screened by the metal electrode. This is a crude but sufficient way of introducing a maximum doping density due to finite ion size effects. The temperature is set at 300 K, the relative dielectric constant at 4. A semiconductor bandgap of 2.4 eV was chosen and ohmic and non-ohmic injection was modeled by setting the electron and hole injection barriers to 0.1 and 1.2 eV, respectively. The applied bias voltage is 3.5 V. The initial homogeneous salt density was set at varying values ranging from 10^{22} to 3×10^{26} nm^{-3}. Optionally, a binding energy between the ions was introduced as explained in Section A.4 of the Supporting Information with varying values for the binding energy E_s and the capture coefficient γ_c (m^3 s^{-1}). Optionally, a doping dependent mobility as described in Section A.3 of the Supporting Information was used with parameters, which were obtained after fitting the doping dependent mobility measured in SY-PPV reported in ref.[9]. Exciton quenching by polarons is described by diffusion-mediated Förster resonance energy transfer.[9] Implementation of this model is as follows. For each time step, an exciton quenching rate is calculated at each grid-point for a given polaron density on the same grid-point. Diffusion of excitons between grid points is included. Diffusion within a grid-point is taken into account via the implemented exciton quenching rate. The polaron density dependent singlet exciton quenching rate k_{PQ} (m^{-3} s^{-1}) is

$$k_{PQ} = \frac{\left[1 - \exp\left(4\pi R_{eff} D_{exc} C_A t_0 - 2.4\sqrt{\pi D_{exc} R_{eff}^2 C_A \sqrt{t_0}}\right)\right]}{t_{step}} \quad (1)$$

where R_{eff} is an effective quenching radius based on the Förster critical radius for quenching, R_0, the exciton lifetime in absence of any quenching, τ_D^o, and exciton diffusion with diffusion constant D_{ex} as described by Valeur [19]

$$R_{eff} = 0.676\left(\frac{R_0^6}{\tau_D^0 D_{ex}}\right)^{1/4} \quad (2)$$

C_A is the acceptor concentration, which is set equal to the sum of the electron and hole densities, and t_0 is the time step taken in the calculation. Note that polarons on neighboring grid-points do not contribute to exciton quenching, which will give rise to some underestimation of the quenching rate. The computational time to reach quasi-steady-state depends on the number of time steps taken. In simulating LEC transients, the transient length is determined by the slowest process, ion redistribution, whereas the maximum time step is determined by the fastest process, related to exciton diffusion and decay. To obtain a reasonable computational time, which is proportional to the ratio of the transient length and the time step, we needed to slow down the fastest processes. The radiative decay rate of the excitons, k_{FL}, and D_{ex} were reduced by a factor 10^{-5}. The resultant delay could, however, give errors in the calculation of the transient behavior of the exciton decay processes. For transients which are limited by the movement of ions care is taken that the ion diffusion coefficient $D_{ion} = \mu_{ion} kT/q$ remains smaller than D_{ex} by at least a factor 10 to minimize this effect.

Supporting Information

Supporting Information is available from the Wiley Online Library or from the author.

Acknowledgements

This work is supported by NanoNextNL, a micro and nanotechnology consortium of the Government of the Netherlands and 130 partners, Project No. NNNL.06D.04.

Received: November 7, 2014
Revised: February 10, 2015
Published online: April 7, 2015

[1] a) Q. B. Pei, G. Yu, C. Zhang, Y. Yang, A. J. Heeger, *Science* **1995**, *269*, 1086; b) Q. B. Pei, Y. Yang, G. Yu, C. Zhang, A. J. Heeger, *J. Am. Chem. Soc.* **1996**, *118*, 3922.
[2] S. van Reenen, P. Matyba, A. Dzwilewski, R. A. J. Janssen, L. Edman, M. Kemerink, *J. Am. Chem. Soc.* **2010**, *132*, 13776.
[3] S. van Reenen, R. A. J. Janssen, M. Kemerink, *Adv. Funct. Mater.* **2012**, *22*, 4547.
[4] a) T. Hu, L. He, L. Duan, Y. Qiu, *J. Mater. Chem.* **2012**, *22*, 4206; b) Y. P. Jhang, H. F. Chen, H. B. Wu, Y. S. Yeh, H. C. Su, K. T. Wong, *Org. Electron.* **2013**, *14*, 2424.
[5] Panasonic news report, http://news.panasonic.com/press/news/official.data/data.dir/2013/05/en130524-6/en130524-6.html (accessed: March 2015).
[6] M. J. Tsai, H. F. Meng, *J. Appl. Phys.* **2005**, *97*, 114502.
[7] H. J. Bolink, E. Coronado, R. D. Costa, N. Lardies, E. Orti, *Inorg. Chem.* **2008**, *47*, 9149.
[8] F. Marchioni, R. Chiechi, S. Patil, F. Wudl, Y. Chen, J. Shinar, *Appl. Phys. Lett.* **2006**, *89*, 061101.
[9] S. van Reenen, M. V. Vitorino, S. C. J. Meskers, R. A. J. Janssen, M. Kemerink, *Phys. Rev. B* **2014**, *89*, 205206.
[10] S. van Reenen, T. Akatsuka, D. Tordera, M. Kemerink, H. J. Bolink, *J. Am. Chem. Soc.* **2013**, *135*, 886.
[11] a) S. B. Meier, D. Hartmann, D. Tordera, H. J. Bolink, A. Winnacker, W. Sarfert, *Phys. Chem. Chem. Phys.* **2012**, *14*, 10886; b) X. Y. Li, J. Gao, G. J. Liu, *Appl. Phys. Lett.* **2013**, *102*, 223303.

© 2015 WILEY-VCH Verlag GmbH & Co. KGaA, Weinheim

[12] a) J. F. Fang, Y. L. Yang, L. Edman, *Appl. Phys. Lett.* **2008**, *93*, 063503; b) J. Fang, P. Matyba, N. D. Robinson, L. Edman, *J. Am. Chem. Soc.* **2008**, *130*, 4562.
[13] N. Kaihovirta, A. Asadpoordarvish, A. Sandstrom, L. Edman, *ACS Photonics* **2014**, *1*, 182.
[14] X. Y. Li, J. Gao, G. J. Liu, *Org. Electron.* **2013**, *14*, 2711.
[15] E. W. Snedden, L. A. Cury, K. N. Bourdakos, A. P. Monkman, *Chem. Phys. Lett.* **2010**, *490*, 76.
[16] D. E. Markov, J. C. Hummelen, P. W. M. Blom, A. B. Sieval, *Phys. Rev. B* **2005**, *72*, 045216.
[17] S. van Reenen, P. Matyba, A. Dzwilewski, R. A. J. Janssen, A. Edman, M. Kemerink, *Adv. Funct. Mater.* **2011**, *21*, 1795.
[18] M. Kuik, L. J. A. Koster, A. G. Dijkstra, G. A. H. Wetzelaer, P. W. M. Blom, *Org. Electron.* **2012**, *13*, 969.
[19] B. Valeur, *Molecular Fluorescence: Principles and Applications*, WILEY-VCH, Weinheim, Germany **2001**.
[20] G. Qian, Y. Lin, G. Wantz, A. R. Davis, K. R. Carter, J. J. Watkins, *Adv. Funct. Mater.* **2014**, *24*, 4484.
[21] S. B. Meier, S. Van Reenen, B. Lefevre, D. Hartmann, H. J. Bolink, A. Winnacker, W. Sarfert, M. Kemerink, *Adv. Funct. Mater.* **2013**, *23*, 3531.

© 2015 WILEY-VCH Verlag GmbH & Co. KGaA, Weinheim